Research Article Vol. 32, No. 26 / 16 Dec 2024 / Optics Express 46322
Optics EXPRESS

Comparison and analysis of methods for measuring the spin transverse relaxation time of rubidium atomic vapor

LULU ZHANG,[1] YONGBIAO YANG,[1] JUNYE ZHAO,[1] YANHUA WANG,[2,3] AND JUNMIN WANG[1,3,*]

[1]State Key Laboratory of Quantum Optics and Quantum Optics Decices, and Institute of Opto-Electronics, Shanxi University, Tai Yuan 030006, Shanxi Province, China

[2]Department of Opto-Electronic Engineering, School of Physics and Electronic Engineering, Shanxi University, Tai Yuan 030006, Shanxi Province, China

[3]Collaborative Innovation Center of Extreme Optics, Shanxi University, Tai Yuan 030006, Shanxi Province, China

[*]wwjjmm@sxu.edu.cn

Abstract: The spin transverse relaxation time (T_2) of atoms is an important indicator for magnetic field precision measurement. Especially in optically-pumped atomic magnetometer, the linewidth of the magnetic resonance signal is one of the most important parameters of sensitivity, which is inversely correlated with T_2 of atoms. In this paper, we propose four methods, namely spin noise spectroscopy signal fitting, radio-frequency free induction decay (RF-FID) signal fitting, ω_m (modulation frequency)-broadening fitting, and magnetic resonance broadening fitting, for in-situ measurement T_2 of atomic vapor cells based on light-atom interactions. Meanwhile, T_2 of three Rubidium (Rb) atomic vapor cells with different parameters are measured and discussed by using these four methods. A comparative analysis visualizes the characteristics of the different methods and the effects of buffer gas on T_2 of Rb atoms. Through theoretical and experimental analysis, we assess the applicability of each method and concluded that the RF-FID signal fitting method provides the most accurate measurements due to the timing sequence control system, which results in a cleaner measurement environment. Furthermore, we demonstrate and qualitatively analyze the relationship between temperature and T_2 of Rb atoms. This work may offer valuable insights into the selection of atomic vapor cells and it is also applicable for the spin-exchange relaxation-free region.

1. Introduction

The precise measurement of magnetic fields has significant application potential in basic physics research [1,2], geophysics [3], clinical medicine [4], and dark matter measurement [5]. The transverse relaxation time (T_2) of atoms is an important indicator to characterize the performance of magnetic field precision measurements. Especially in optically-pumped atomic magnetometer [6–8], the linewidth of the magnetic resonance signal is one of the most important indicators of sensitivity, which is inversely correlated with T_2 of atoms. For example, the spin-exchange relaxation-free (SERF) magnetometer [9] has the highest magnetic field sensitivity, its magnetic resonance linewidth is about 40-60 Hz, the relaxation time is about 20 ms [10–13]. For other types of magnetometers, previous studies have demonstrated that magnetometers that tend to have longer T_2 generally have higher magnetic field sensitivity, so the T_2 of atoms focused on by researchers when atomic vapor cells are customised. Because of this, it is necessary to accurately measure T_2 of atoms to help select the ideal type of atomic vapor cell.

Currently, the traditional free induction decay (FID) method is a commonly used method for measuring T_2 of atoms. Z. C. Ding *et al* [14] investigated the influences of linearly polarized

#542760 https://doi.org/10.1364/OE.542760
Journal © 2024 Received 20 Sep 2024; revised 8 Nov 2024; accepted 14 Nov 2024; published 6 Dec 2024

Optics EXPRESS

light at Cesium (Cs) on the transverse relaxation of ground–state Cs atoms based on FID method. D. X. Bai *et al* [15] propose an intelligent algorithm for measuring the relaxation time of the Bell-Bloom magnetometer parameters. Besides, P. Jiang *et al* [16] proposed the fitting-ratio method and the magnetic resonance broadening method to measure T_2 of atoms, and compared with the traditional FID method to explore the advantages of the new methods. And in 2020, the group proposed a perturbation-free method to measure T_2 [17] of atoms in a nuclear magnetic resonance oscillator. In 2023, M. M. Wei *et al* [18] measured T_2 of Cs based on the principle of longitudinal field modulation.

In addition, the spin noise spectrum signal in the spin noise spectroscopy technique also contains a significant amount of information and is an important method for the measurement of T_2. In 2007, G. E. Katsoprinakis et al [19] analyzed the spin noise spectroscopy properties of atoms in detail from theoretical and experimental perspectives, revealing the relationship between the spin spectrum and T_2 of atoms.

Although each of the aforementioned measurement methods has its own merits, in practial applications, the implementation of a simple and efficient approach for measuring T_2 can conserve space and reduce costs , warranting futher comparative analysis. In this paper, we propose four methods for in-situ measurement T_2 of atomic vapor cells based on light-atom interactions. First, The atomic relaxation time is introduced, and the formula for deriving the relaxation time by four methods (spin noise spectroscopy fitting, radio-frequency free induction decay (RF-FID) signal fitting, ω_m (modulation frequency)-broadening fitting, and magnetic resonance broadening fitting) is obtained. second, experiments are conducted to measure T_2 of Rubidium (Rb) atoms by four methods. Thirdly, the impact and results of system in the experiments is analyzed and discussed in detail. Meanwhile, T_2 of three Rb atomic vapor cells with different parameters available in our laboratory were analyzed by using the above four measurement methods, to visually observe the merits of various methods and the effects of different types of buffer gases on T_2 of Rb atoms. Finally, the relationship between temperature and T_2 was verified by experimentally measuring a typical Rb atomic vapor cell.

2. Theoretical analysis

The relaxation time of an atom is divided into the longitudinal relaxation time (T_1) and the transverse relaxation time (T_2). Longitudinal relaxation is the relaxation of the atomic state population to a certain equilibrium value, which is related to the spin of the atom, that is, the lifetime of the atomic state. Transverse relaxation is phase-dependent and refers to the decoherence time of phase.

For alkali metal atomic ensembles, under the action of the static magnetic field B_z along the z-axis, the components of macroscopic magnetization of atoms in thermal equilibrium are:

$$\begin{aligned} M_z &= M_0, \\ M_x &= M_y = 0. \end{aligned} \tag{1}$$

Here M_0 is a constant value. If a pump light is simultaneously applied along the z-axis to polarize the alkali metal atoms, an oscillating magnetic field with amplitude B_1, frequency Ω is introduced, whose direction is perpendicular to the static magnetic field B_z, to deflect the spin polarization of the alkali metal atoms away from the z-axis. Then the pump light and the oscillating magnetic field are withdrawn, the alkali metal atoms are in a non-equilibrium state, and some relaxation mechanism restores it to a thermal equilibrium state. In a rotating coordinate system, the evolution of the macroscopic magnetization of alkali metal atoms can be expressed

Optics EXPRESS

by the Bloch equation, which is described as follows [20]:

$$\begin{aligned} \frac{dM'_x(t)}{dt} &= \Delta\omega M'_y(t) - \frac{M'_x(t)}{T_2}, \\ \frac{dM'_y(t)}{dt} &= \gamma B_1 M_z(t) - \Delta\omega M'_x(t) - \frac{M'_y(t)}{T_2}, \\ \frac{dM_z(t)}{dt} &= -\gamma B_1 M'_y(t) + \frac{M_0 - M_z(t)}{T_1}. \end{aligned} \tag{2}$$

Here, $\Delta\omega = \omega_L - \Omega$ is the mismatch between the Larmor frequency ω_L and the oscillating magnetic field frequency Ω, and γ is the ground-state gyromagnetic ratio. In this process, the macroscopic magnetization of alkali metal atoms is decomposed into a component M_z (parallel to the static magnetic field) and components M_x, M_y (perpendicular to the static magnetic field). The characteristic time from M_z to M_0 is referred to as T_1. The characteristic time for M_x and M_y to gradually return to 0 is called T_2, in which the spin precession phase of the alkali metal atoms is redistributed until it is disordered.

For an atomic magnetometer, the relationship between its sensitivity and T_2 is [21]:

$$\delta B = \frac{1}{\gamma\sqrt{n_{al} T_2 V t}} \tag{3}$$

Here n_{al} is the density of atoms, V is the cell volume, t is the measurement time. So measuring T_2 is critical for calculating the sensitivity of magnetometers.

2.1. Spin noise spectroscopy fitting

Spin noise is the random distribution of atomic electron spins in quasi-thermodynamic equilibrium. The spin noise spectroscopy is an optical technique that can be obtained from nuclear magnetic resonance measurements and magnetic force microscopy measurements; however, the most sensitive and widely used detection technique is Faraday rotation, which maps atomic spin noise on the polarization plane of a non-resonant probe light. Furthermore, we experimentally measured and analyzed the spin noise spectrum of Rb in previous articles [22,23], and have a certain understanding of its principle and parameter optimization.

Based on the principle of the spin noise spectroscopy, the spin noise spectrum signal of Voigt configuration correlate with T_2. The light beam is perpendicular to the static magnetic field, the random fluctuation of magnetization process around the direction of the static magnetic field, and this fluctuation on the spectrum manifests as Lorentzian-linear peak. The half width at half maximum (HWHM) of the peak is inversely correlated with T_2 [24,25]. Moreover, the experimental setup used in our apparatus employed this method to measure T_2.

2.2. RF-FID signal fitting

In RF-FID magnetometer, the direction of the pump light is parallel to the static magnetic field, and an oscillating magnetic field with the Larmor frequency is used for $\pi/2$ pulse times [26,27]. These cause the macroscopic magnetization of the atomic ensemble in a plane perpendicular to the static magnetic field, and the precession is exponentially attenuated around the static magnetic field at the Larmor frequency. This Larmor precession is mapped to the rotation of the probe light polarization plane, and the FID signal is subsequently detected with a differential detector.

Here, we employ a timing sequence control system to ensure that only far-detuned probe light and static magnetic field are present during FID signal detection. This approach has been thoroughly analyzed and experimentally measured in our previous work [28]. The RF-FID magnetometer can mitigate issues related to measurement accuracy caused by the disruption of spin polarization by pump light and RF magnetic field.

Optics EXPRESS

For an FID signal with amplitude of A_{FID} , by extracting the evolution of the FID signal and fitting it accordingly, T_2 of atoms can be obtained [29,30] :

$$S_{FID} = A_{FID} exp(-t/T_2) sin(\omega_L t) \tag{4}$$

2.3. ω_m-broadening fitting

In this method, a modulated magnetic field with frequency ω_m is applied in the direction of the static magnetic field B_z. If there are magnetic fields B_x and B_y considerable smaller than static magnetic field B_z exists in the x and y directions, the expression of the in-phase and quadrature phase signals after lock-in amplifier (LIA) demodulation is [18]:

$$\begin{aligned} S_{IS} &\propto \frac{B_y - B_x(\gamma B_z + n\omega_m)T_2}{1 + {T_2}^2 (\gamma B_z + n\omega_m)^2}, \\ S_{QS} &\propto \frac{B_x - B_y(\gamma B_z + n\omega_m)T_2}{1 + {T_2}^2 (\gamma B_z + n\omega_m)^2}. \end{aligned} \tag{5}$$

where n is the ratio of the Larmor frequency ω_L to the modulation frequency ω_m, i.e., $n = \omega_L$ / ω_m. When $B_x \neq 0$, $B_y = 0$, the above equation can be written as:

$$\begin{aligned} S_{IS} &\propto \frac{-B_x(\gamma B_z + n\omega_m)T_2}{1 + {T_2}^2 (\gamma B_z + n\omega_m)^2}, \\ S_{QS} &\propto \frac{B_x}{1 + {T_2}^2 (\gamma B_z + n\omega_m)^2} \end{aligned} \tag{6}$$

Similarly, we can find the in-phase and quadrature phase signals of the LIA demodulation in case $B_x = 0$, $B_y \neq 0$. From the above equation, the relationship between HWHM (Γ) and T_2 can be obtained: $\Gamma_{QS} = \Gamma_{IS} = 1/ (nT_2)$.

2.4. Magnetic resonance broadening fitting

In this method, an RF magnetic field with magnitude B_1, frequency Ω is applied perpendicular to the direction of the static magnetic field. In a rotating coordinate system, the steady-state solution of the magnetization M is [31] :

$$\begin{aligned} M'_x &= \frac{M_0 \gamma B_1 \Delta\omega}{(1/T_2)^2 + (\Delta\omega)^2 + (T_1/T_2)(\gamma B_1)^2}, \\ M'_y &= \frac{M_0 \gamma B_1 (1/T_2)}{(1/T_2)^2 + (\Delta\omega)^2 + (T_1/T_2)(\gamma B_1)^2}, \\ M_z &= \frac{M_0[(\Delta\omega)^2 + (1/T_2)^2]}{(1/T_2)^2 + (\Delta\omega)^2 + (T_1/T_2)(\gamma B_1)^2}. \end{aligned} \tag{7}$$

Scanning the static magnetic field B_0, the relationship between HWHM and B_1 after LIA demodulation is [16] :

$$\Gamma = \sqrt{(1/T_2)^2 + (T_1/T_2)(\gamma B_1)^2} \tag{8}$$

And $\Gamma = 1/T_2$ when the RF magnetic field strength is sufficiently small to be negligible.

3. Experimental setup

Our experimental setup is shown in Fig. 1, in which a cubic ^{87}Rb enriched atomic vapor cell, contains 100 Torr N_2, with a size of 15 mm × 15 mm × 15 mm is used for the experiment. The AC-driven non-magnetic heating films and servo loop act as a heating system to control the

Optics EXPRESS

temperature of the atomic vapor cell at 75 °C. The cell is housed within four layers of μ-metal magnetic shielding to shield the ambient magnetic field. The three-axis Helmholtz coil is placed inside to generate the magnetic field, where the direction of the static magnetic field B_0 is along the z-axis, and the static magnetic field B_0 is 6.32 μT.

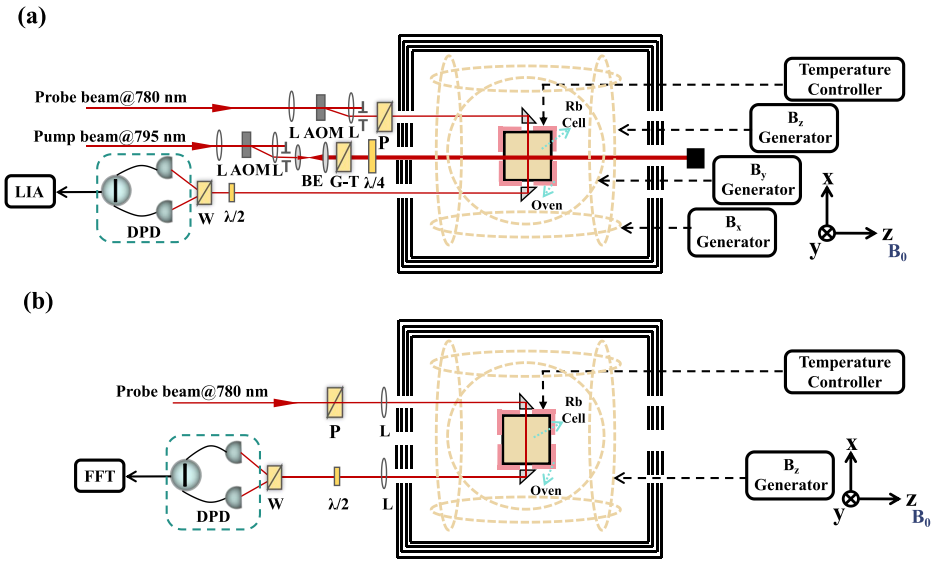

Fig. 1. (a) Schematic diagram of Rb atomic magnetometer setup. (b) Schematic diagram of spin noise spectroscopy scheme. AOM: acousto-optic modulator; BE: beam expander; λ/4: quarter-wave plate; λ/2: half-wave plate; G-T: Glan Taylor prism; L: lens P: polarizer; W: Wollaston prism; DPD: differential photodetector; LIA: lock-in amplifier; FFT: fast Fourier transform.

The magnetometer configuration is shown in Fig. 1 (a). The pump light provided by the 795-nm external cavity diode laser (ECDL) passes through the acousto-optic modulator (AOM), beam expander, Glan-Taylor prism, and quarter-wave plate into a circularly polarized pumped light with a beam diameter of ~ 10 mm, and then enters the Rb atomic vapor cell along the z-axis. In the experiment, depending on the type of atomic vapor cell, the frequency of the pump light is locked at ^{87}Rb D1 line (F=2)-(F'=1) transition. The pump light intensity entering the cell is 12.7 mW/cm^2. The probe light from the 780-nm distributed-Bragg-reflector (DBR) diode laser passes through the AOM and the polarizer to become linearly-polarized light with a beam diameter of ~ 2 mm. The frequency of the probe light is blue detuned 18 GHz from ^{87}Rb D2 line (F=2)-(F'=2) transition, and the light intensity entering the cell is 3.2 mW/cm^2. After traversing the cell along the x-axis, the probe light enters a balanced polarimeter where the optical signal is converted into an electrical signal and fed into the LIA.

For the spin noise spectroscopy configuration, as shown in Fig. 1 (b), the direction of the static magnetic field is along the z-axis. Only a 780-nm linearly-polarized probe beam is used to traverse the vapor cell along the x-axis, the diameter of the minimum beam waist after passing through the lens is ~ 0.25 mm. The rotation of the probe light polarization is received by the balanced polarimeter, subsequently into the fast Fourier transform (FFT) to convert the time-domain signal into a frequency-domain signal.

Optics EXPRESS

4. Results and discussion

4.1. Measurement results and analysis of the four methods

In the spin noise spectroscopy fitting method, the static magnetic field B_0 is 6.32 μT, and the probe power is 100 μW. Due to the spin noise spectrum originating from unpolarized atoms, to obtain a more distinct spin noise spectrum signal, we focused the probe beam. The typical spin noise spectrum signal after FFT is shown in Fig. 2. We set the average sample number to 1000 times, and obtained the HWHM of 751 Hz by Lorentz fitting.

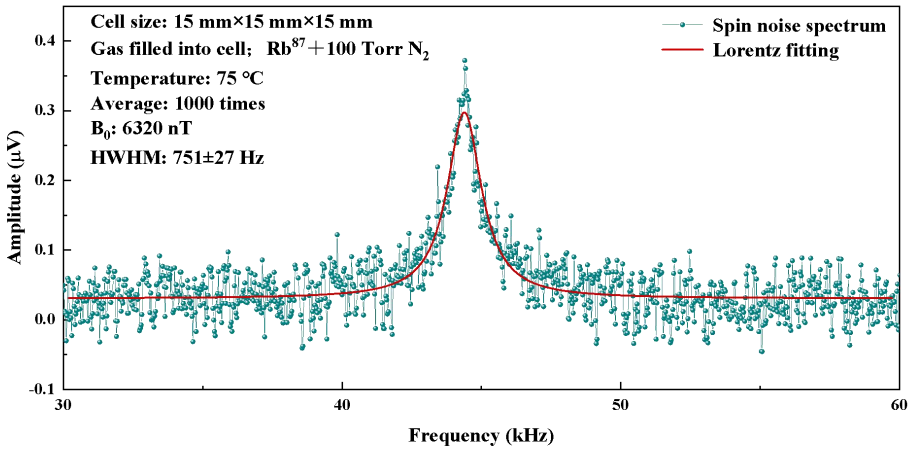

Fig. 2. Spin noise spectroscopy signal. The red curve is the Lorentz fitting, with a typical HWHM of 751 Hz. Other parameters: cell: ^{87}Rb + 100 Torr N_2; Temperature: 75°C; the frequency of the probe beam power is blue detuning 10 GHz from ^{87}Rb D2 line (F=2)-(F'=2) transition. The spin noise spectrum is averaged 1000 times and B_0 is 6.32 μT.

In the RF-FID signal fitting method, our timing sequence control system based on AOM is shown in the inset of Fig. 3 (a), to separate the pump light, RF magnetic field, and probe light from the time domain, as well as to avoid the influence of crosstalk between the three on the FID signal [28]. Here, we set the typical timing sequence as 5 ms for the pump light time, 3 mA for the current to apply the RF magnetic field strength, the corresponding $\pi/2$ pulse time of 0.2 ms, and the detection time of 14.8 ms. The typical experimental result is shown in Fig. 3, and T_2 of Rb atoms is 3.682 ms.

Based on the RF-FID mode, we measure a series of cycles to get the magnetic field data, and then calculate the magnetometer sensitivity by the power spectral density of magnetic field noise as shown in Fig. 3 (b), and the magnetometer sensitivity in the range of 1-25 Hz is 5.2 pT/Hz$^{1/2}$. In our experiment, one reason the sensitivity did not exceed the pT level may be due to the attenuation of pump light intensity in the atomic vapor cell. This attenuation can lead to spatial inhomogeneity and light shifts, resulting in inconsistencies in the accuracy and sensitivity experienced by each probe channel of the differential output [32]. To address this issue, future work could explore the use of counter-propagating of pump light to mitigate these effects [33]. On the other hand, the fact that the coils generating the static magnetic field are manually wound may contribute to the magnetic field gradient, may also be a factor contributing to the reduction in sensitivity.

In ω_m - broadening fitting method, we set the frequency ω_m of the modulation field to half the Larmor frequency ω_L, i.e. n=2, and sweep the frequency near the modulated frequency. Set B_x = 0.41 μT, B_y = 0 μT or B_x = 0 μT, B_y = 0.41 μT. The typical in-phase and quadrature

Optics EXPRESS

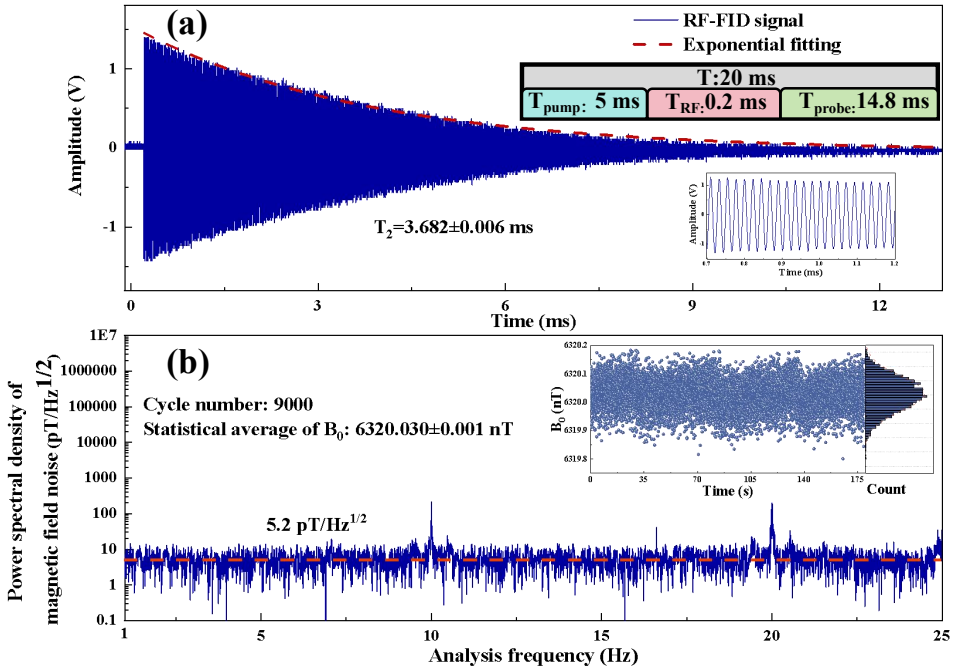

Fig. 3. (a) The RF-FID signal. The red dotted line is the exponential fitting. Inset: timing sequence control system (top) and several FID precession cycles (bottom). (b) The sensitivity of optically pump Rb magnetometer obtained by power spectral density of magnetic field noise calculation in FID mode. Inset: Magnetic field data recorded from 9000 measurement cycles. The red curve is a Gaussian fitting.

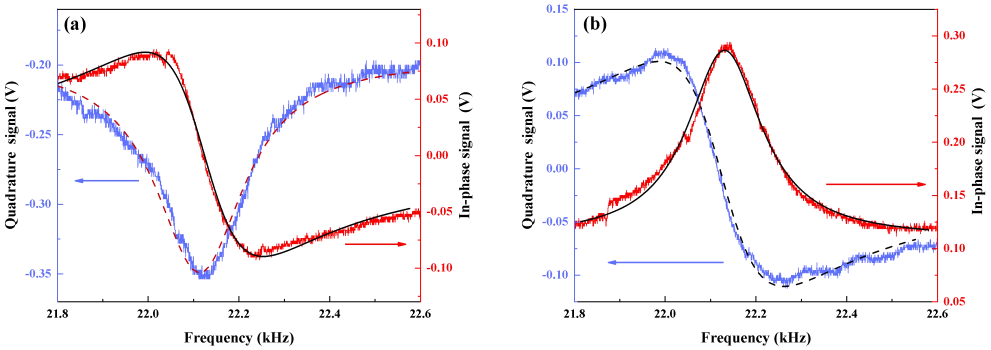

Fig. 4. (a) The demodulated in-phase and quadrature signals when $B_x = 0.41$ μT, $B_y = 0$ μT. (b) The demodulated in-phase and quadrature signals when $B_x = 0$ μT, $B_y = 0.41$ μT.

signals obtained by LIA are shown in Fig. 4, where ω_m is also the reference frequency of LIA, the extracted T_2 of Rb atoms is 3.921 ms.

In magnetic resonance broadening fitting methods, we apply an RF magnetic field with a frequency equal to the Larmor frequency on the y-axis, and the reference signal frequency demodulated by the LIA is set to the Larmor frequency. By scanning the static magnetic field applied on the z-axis, the in-phase and quadrature signals are shown in Fig. 5 (a). The HWHM is obtained by Lorentz fitting of the demodulated signal. With the change of RF magnetic

Optics EXPRESS

field strength, the variation of HWHM with RF magnetic field strength is shown in Fig. 5 (b). According to Eq. (8), T_2 of Rb atoms is 2.952 ms.

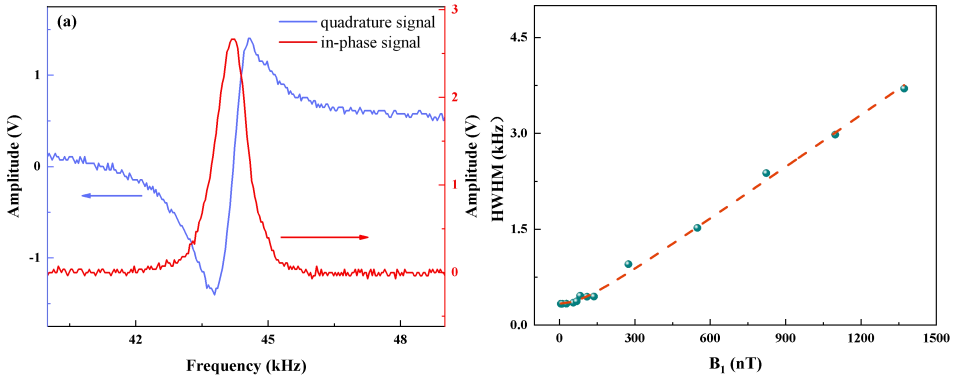

Fig. 5. (a) The in-phase and quadrature signals while B_1 = 69 nT. (b) Dependence between HWHM and RF magnetic field strength.

4.2. *Comparison and analysis of different rubidium vapor cells*

Furthermore, considering the atomic vapor cell in hand, three types of Rb atomic vapor cells are used in the above four methods to measure T_2 of Rb atoms, the parameters of which are shown in Table 1. Among the four measurement methods, the pump beam parameter in the spin noise spectroscopy fitting method significantly differ from those of the other three due to the distinct nature of the measurement methods. In the spin noise spectroscopy fitting, to obtain a distinct signal, we employ lens to focus the probe beam, resulting in higher light intensity, particularly at the smallest beam waist where the intensity is maximized. Power broadening is thus a factor that warrants consideration. Moreover, the detuning of the probe beam is relatively smaller compared to the other three methods, which, for our vapor cells filled with a large amount of buffer gas, makes power broadening an important consideration. Based on this, as stated in the Ref. [19], we acquired spin noise spectrum corresponding to a range of power values and fitted them to obtain the respective T_2 values. Subsequently, we employed linear extrapolation to determine the T_2 value at near-zero probe light intensity, in order to address the issue of power broadening. As indicated by Fig. 6 and Table 3, the T_2 values obtained through the spin noise spectroscopy fitting method, after simply addressing the power broadening issue, do not show significant differences compared to the other three methods. It suggests that power broadening maybe a prominent dominant factor in spin noise spectrum measurements. Certainly, subsequent studies could explore the influence of beam waist on both the spin noise spectrum and T_2 values.

Table 1. Nominal parameters of the three rubidium atomic vapor cells

Cell number	Cell size (mm)	Gas filled into cell
#1	15×15×15	^{87}Rb+100 Torr N_2
#2	20×20×20	Natural abundance (^{87}Rb+^{85}Rb)+100 Torr N_2
#3	20×20×20	Natural abundance (^{87}Rb+^{85}Rb)+600 Torr N_2+50 Torr He

Additionally, the spin noise spectroscopy fitting method measures atomic spins' fluctuations under unpolarization, which yields a relatively small signal amplitude and a poor signal-to-noise ratio, and the prolonged measurement time still limited the T_2 value that we could measure [19,24], this also have a certain impact on the precision of the measurements.

Optics EXPRESS

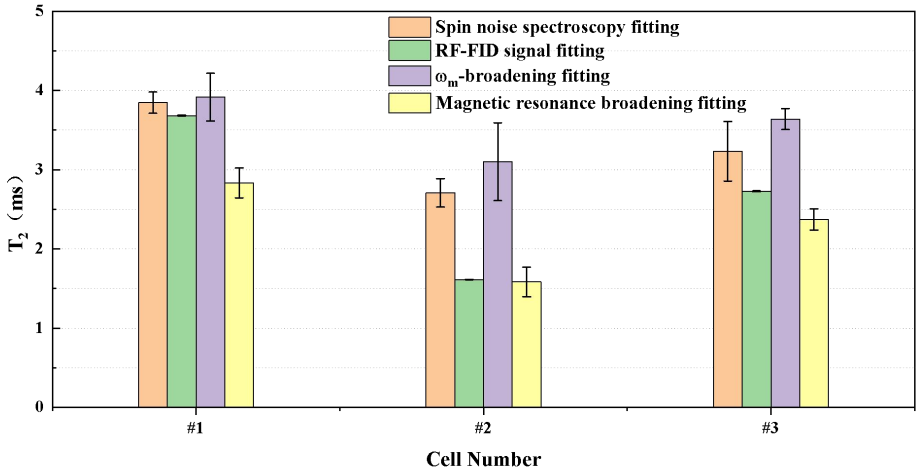

Fig. 6. T_2 of Rb atoms measured by spin noise spectroscopy fitting, RF-FID signal fitting, ω_m - broadening fitting, and magnetic resonance broadening fitting, in different Rb vapor cells. For the RF-FID signal fitting, the error bar is small enough to be submerged in the columnar bar. The temperature of Rb vapor cell is controlled at 75°C.

For the other three methods, the beam parameters in the experimental setup were essentially the same, involving pumping beam for atomic spin polarization and probe beam for signal detection. Since the frequency of the probe beam is far-detuned and the intensity is sufficiently low, we believe that the issue of power broadening caused by the probe beam in these three methods can be neglected. For the RF-FID fitting method, in contrast to the other two methods, ensures there is no interference from the pumping beam and RF magnetic field through a timing sequence control system. Only a static magnetic field is present, causing the spin-polarized atoms to undergo spin free induction decay precession around it, which is then mapped onto the polarization plane of the probe beam and detected as a rotational signal by a differential detector. In contrast, the magnetic resonance broadening fitting method involves the coexistence of both pump beam and RF magnetic field during the measurement process. Furthermore, the ω_m-broadening fitting method also introduces an additional magnetic field, this could lead to crosstalk between the fields, potentially affecting the accuracy of the measured T_2 values, causing them to deviate more significantly. Taking these factors into account, among the four methods, we contend that the RF-FID fitting method, which is less perturbed during measurement, yields T_2 values that are closer to the true values and thus has higher accuracy.

Meanwhile, Fig. 6 and Table 2 reveal that among the four methods, the spin noise spectroscopy fitting, the ω_m-broadening fitting method and the magnetic resonance broadening fitting method exhibit relatively larger errors during measurement. The RF-FID method, conversely, has the smallest error, indicating a higher precision in the measurement process.

Table 2. T_2 values of different Rb atomic vapor cells obtained by four methods in 75 °C

Measurement method \ Cell number	#1 cell	#2 cell	#3 cell
Spin noise spectroscopy fitting	3.846 ± 0.134 ms	2.708 ± 0.179 ms	3.233 ± 0.376 ms
RF-FID signal fitting	3.682 ± 0.006 ms	1.413 ± 0.002 ms	2.728 ± 0.006 ms
ω_m-broadening fitting	3.916 ± 0.301 ms	3.101 ± 0.492 ms	3.640 ± 0.130 ms
Magnetic resonance broadening fitting	2.834 ± 0.188 ms	1.284 ± 0.187 ms	2.372 ± 0.134 ms

Optics EXPRESS

Additionally, within a specific temperature range, the buffer gas primarily suppresses the rate of spin-destructive collisions [34,35]. The type and pressure of the buffer gas used can vary, resulting in different T_2 values. For the #2 Rb vapor cell and #3 Rb vapor cell, the buffer gas in #3 Rb vapor cell exhibits a more effective suppression of spin-destructive collisions.

T_2 values of the #1 Rb vapor cell with different atomic number densities (different temperatures) measured by using of the RF-FID scheme, and typical results are shown in Table 3. Here, the atomic number density n_a can be determined by $n_a = 133.3p/(k_BT)$, p is pressure, k_B is the Boltzmann constant, and T is atomic vapor cell temperature [36]. T_2 of Rb atoms is inversely related with atomic number density. The relaxation mechanism affecting T_2 can be given by [31,37]:

Table 3. T_2 values of the #1 Rb vapor cell with different atomic number densities (different temperatures) measured by using of the RF-FID scheme

Temperature(°C)	atomic density(atoms/cm^3)	T_2 (ms)
65	5.03×10^{11}	5.245± 0.014
70	7.04×10^{11}	5.022± 0.006
75	1.08×10^{12}	3.628± 0.006
80	1.55×10^{12}	3.211± 0.005
85	2.21×10^{12}	2.646± 0.008
90	3.11×10^{12}	2.136± 0.012

$$\frac{1}{T_2} = \frac{1}{q}(R_{SD} + R_{OP} + R_{PR}) + R_{wall} + \frac{1}{q_{SE}}R_{SE} + R_{gr} \tag{9}$$

$R_{SD} = \sum_i n_i \bar{v}_{ij} \sigma_{ij}$ is the rate of relaxation due to spin-destruction collisions, i and j represent different atomic species, n_i is the atomic density of atom, $\bar{v}_{ij}$ is the relative thermal velocity between atoms, σ_{ij} is the effective collisional cross-section, $R_{SE} = n_{Rb}\bar{v}\sigma_{SE}$ is the rate of spin-exchange collisions between alkali atoms, R_{OP} is the optical pumping rate, R_{PR} is the absorption rate of photons from the probe beam, R_{wall} is the rate of depolarization due to collisions with the wall of the vapor cell, q is the nuclear slowing-down factor, q_{SE} is the spin-exchange broadening factor, and R_{gr} is the broadening due to the magnetic field gradient across the vapor cell.

For the RF-FID scheme, during the measurement period, the pumping beam is turned off, causing no relaxation. Additionally, due to the far-detuned and weak intensity of the probe beam, R_{PR} can also be ignored [13]. The spin-destruction relaxation rate and the spin-exchange relaxation rate increase with temperature, but the relaxation due to spin-destruction collisions and collisions with the wall of the vapor cell is suppressed to a certain extent by the filling with buffer gas, and therefore is mainly affected by the relaxation of spin-exchange collisions as the atomic number density increases [31].

However, the increasing number density of rubidium atoms leads to a faster increase in the signal amplitude of the magnetic resonance signal. Therefore, it is still possible to obtain better signal-to-noise ratios of the magnetic resonance signals at optimized higher temperatures, thus making it possible to achieve an improvement in the sensitivity of optically pumped atomic magnetometers.

Generally, spin-exchange collisions can be further suppressed by optical narrowing effects [38–40] or by heating the atomic vapor cell to extremely high temperature to keep atoms in the SERF state [41]. Although , SERF magnetometer also necessitate a weaker ambient magnetic field [10].

Optics EXPRESS

5. Conclusions

In conclusion, four methods for in-situ measurement of T_2 of atomic vapor cells based on light-atom interactions are proposed and experimentally performed, and the formula for deriving the spin transverse relaxation time T_2 by four methods is obtained. T_2 of three Rb atomic vapor cells with different parameters available in our laboratory were analyzed by using the above four measurement methods. We demonstrate the dependence between different temperatures and T_2 of Rb atoms in the RF-FID scheme, and conducted an analysis of the relaxation mechanism.

In the spin noise spectroscopy fitting method, the probe beam power broadening is a major dominant factor. Moreover, the requirement for high-resolution spin noise spectroscopy technique and longer measurement times are also among the limitations for obtaining accurate T_2 values. The experimental setup for the magnetic resonance broadening fitting method is relatively simple. It is easier to implement experimentally, and even T_2 of atoms can be measured only by measuring the pump light [15]. The ω_m - broadening fitting method allows real-time monitoring of the drift of the static magnetic field, which can be compensated by a servo-loop system. Although the experimental setup for the RF-FID signal fitting method is relatively complex, it ensures that the negative effects of the RF magnetic field and pump light are not introduced during the measurement, T_2 of atoms measured by this method is relatively accurate.

These four methods can be used in different measuring environments. T_2 of atoms obtained by different measuring methods are slightly different, mainly because each method imposes distinct requirements on the experimental apparatus, leading to dissimilar beam parameters and magnetic field environments during measurement. However, all of them intuitively show the relationship between the buffer gases of different pressures and T_2. This provides a variety of feasible methods for future precision measurement fields, especially in optically-pumped atomic magnetometers. Moreover, although our experiments did not achieve the SERF region, we believe that our measurement method is also applicable in the SERF region [42]. We can further calibrate the magnetic field sensitivity by measuring T_2 of atoms to characterize the linewidth of the magnetic resonance signal. This study also has important application reference value in the fields of the fabrication of atomic vapor cells, and the selection of buffer gas types and pressures. Disclosures. The authors declare no conflicts of interest. Data availability. Data underlying the results presented in this paper may be available from the corresponding author upon reasonable request.

Funding. National Natural Science Foundation of China (12474483, 11974226); Fundamental Research Program of Shanxi Province (202403021211013); 1331 Key Subjects Construction project of Shanxi Province, China.

Disclosures. The authors declare that there are no conflicts of interest related to this article.

Data availability. Data underlying the results presented in this paper are not publicly available at this time but may be obtained from the authors upon reasonable request.

References

1. S.-K. Lee, K. L. Sauer, S. J. Seltzer, *et al.*, "Subfemtotesla radio-frequency atomic magnetometer for detection of nuclear quadrupole resonance," Appl. Phys. Lett. **89**(21), 214106 (2006).
2. J. M. Brown, S. J. Smullin, T. W. Kornack, *et al.*, "New limit on Lorentz- and CPT-violating neutron spin interactions," Phys. Rev. Lett. **105**(15), 151604 (2010).
3. M. N. Nabighian, V. J. S. Grauch, R. O. Hansen, *et al.*, "The historical development of the magnetic method in exploration," Geophysics **70**(6), 33ND–61ND (2005).
4. R. Zhang, W. Xiao, Y. D. Ding, *et al.*, "Recording brain activities in unshielded earth's field with optically pumped atomic magnetometers," Sci. Adv. **6**(24), eaba8792 (2020).
5. M. Jiang, H. W. Su, A. Garcon, *et al.*, "Search for axion-like dark matter with spin-based amplifiers," Nat. Phys. **17**(12), 1402–1407 (2021).
6. H. Crepaz, L. Y. Ley, and R. Dumke, "Cavity enhanced atomic magnetometry," Sci. Rep. **5**(1), 15448 (2015).
7. Q. Q. Guo, T. Hu, C. Q. Chen, *et al.*, "A high sensitivity closed-loop spin-exchange relaxation-free atomic magnetometer with broad bandwidth," IEEE Sens. J. **21**(19), 21425–21431 (2021).
8. X. J. Liu, Y. Li, X. D. Wu, *et al.*, "Reflected atomic magnetometer with single beam," IEEE Sens. J. **22**(2), 1238–1244 (2022).

Optics EXPRESS

9. Y. T. Xu, Z. Chai, J. Sun, *et al.*, "A Miniaturized Spin-Exchange Relaxation-Free Atomic Magnetometer Array Based on a 1×8 Planar Lightwave Circuit Waveguide Splitter," Adv. Quantum Technol. **6**(8), 2300084 (2023).
10. I. K. Kominis, T. W. Kornack, J. C. Allred, *et al.*, "A subfemtotesla multichannel atomic magnetometer," Nature **422**(6932), 596–599 (2003).
11. H. B. Dang, A. C. Maloof, and M. V. Romalis, "Ultrahigh sensitivity magnetic field and magnetization measurements with an atomic magnetometer," Appl. Phys. Lett. **97**(15), 151110 (2010).
12. M. Jiang, R. P. Frutos, T. Wu, *et al.*, "Magnetic Gradiometer for the Detection of Zero- to Ultralow-Field Nuclear Magnetic Resonance," Phys. Rev. Appl. **11**(2), 024005 (2019).
13. J. Peng, A. N. Xu, Y. Yin, *et al.*, "Measurement of Relaxation Mechanism for the Spin-Exchange Relaxation-Free Magnetometer," IEEE Sens. J. **24**(2), 1333–1339 (2024).
14. Z. C. Ding and J. Yuan, "Influence of linearly polarized light on the transverse relaxation of ground-state ^{133}Cs atoms," Sci. Rep. **14**(1), 12404 (2024).
15. D. X. Bai, L. H. Cheng, Y. Z. Sun, *et al.*, "RT-FPS: Relaxation time of free precession signal measurement method for Bell-Bloom magnetometer," IEEE Trans. Geosci. Remote Sensing **62**, 1–15 (2024).
16. P. Jiang, Z. G. Wang, and H. Luo, "Techniques for measuring transverse relaxation time of xenon atoms in nuclear-magnetic-resonance gyroscopes and pump-light influence mechanism," Optik **138**, 341–348 (2017).
17. C. Chen, Q. Y. Jiang, Z. G. Wang, *et al.*, "A non-interference method for measurement of transverse relaxation time of the alkali metal magnetometer in nuclear magnetic resonance oscillator," AIP Adv. **10**(6), 065303 (2020).
18. M. M. Wei, W. B. Yu, M. Zhou, *et al.*, "Three techniques for measuring the transverse relaxation time of cesium atoms," AIP Adv. **13**(3), 035327 (2023).
19. G. E. Katsoprinakis, A. T. Dellis, and I. K. Kominis, "Measurement of transverse spin-relaxation rates in a rubidium vapor by use of spin-noise spectroscopy," Phys. Rev. A **75**(4), 042502 (2007).
20. F. Bloch, "Nuclear induction," Phys. Rev. **70**(7-8), 460–474 (1946).
21. J. C. Allred, R. N. Lyman, T. W. Kornack, *et al.*, "High-sensitivity atomic magnetometer unaffected by spin-Exchange relaxation," Phys. Rev. Lett. **89**(13), 130801 (2002).
22. Y. L. Yang, L. L. Bai, L. L. Zhang, *et al.*, "Experimental investigation of spin noise spectroscopy of rubidium atomic ensemble," Acta Phys. Sin. **69**(23), 233201 (2020).
23. L. L. Bai, L. L. Zhang, Y. B. Yang, *et al.*, "Enhancement of spin noise spectroscopy of rubidium atomic ensemble by using the polarization squeezed light," Opt. Express **30**(2), 1925–1936 (2022).
24. V. S. Zapasskii, "Spin-noise spectroscopy: from proof of principle to applications," Adv. Opt. Photonics **5**(2), 131–168 (2013).
25. J. Hübner, F. Berski, R. Dahbashi, *et al.*, "The rise of spin noise spectroscopy in semiconductors: from acoustic to GHz frequencies," Phys. Status Solidi B **251**(9), 1824–1838 (2014).
26. C. Liu, H. Dong, and J. Sang, "Submillimeter-resolution magnetic field imaging with digital micromirror device and atomic vapor cell," Appl. Phys. Lett. **119**(11), 114002 (2021).
27. S. G. Li, J. S. Liu, M. Jin, *et al.*, "A kilohertz bandwidth and sensitive scalar atomic magnetometer using an optical multipass cell," Measurement **190**, 110704 (2022).
28. L. L. Zhang, Y. B. Yang, N. Zhao, *et al.*, "A multi-Pass optically pumped rubidium atomic magnetometer with free induction decay," Sensors **22**(19), 7598 (2022).
29. H. B. Dong, H. Liu, J. Ge, *et al.*, "A high-precision frequency measurement algorithm for FID signal of proton magnetometer," IEEE Trans. Instrum. Meas. **65**(4), 898–904 (2016).
30. H. Li, M. I. Jiang, Z. N. Zhu, *et al.*, "Calibration of magnetic field measurement capability of rubidium-xenon vapor cell atomic magnetometer," Acta Phys. Sin. **68**(16), 160701 (2019).
31. D. Budker and D. F. Jackson Kimball, *Optical magnetometry* (Cambridge University Press, 2013).
32. T. Moriyasu, D. Nomoto, Y. Koyama, *et al.*, "Spin Manipulation Using the Light-Shift Effect in Rubidium Atoms," Phys. Rev. Lett. **103**(21), 213602 (2009).
33. J. Peng, A. -N. Xu, and B. Liu, "Femtotesla atomic magnetometer with counter-propagating optical sideband pumping," Opt. Lett. **49**(21), 6177 (2024).
34. M. V. Romalis, E. Miron, and G. D. Cates, "Pressure broadening of Rb D1 and D2 lines by ^{3}He, ^{4}He, N_2, and Xe: Line cores and near wings," Phys. Rev. A **56**(6), 4569–4578 (1997).
35. Y. X. Wang, G. Jin, J. J. Tang, *et al.*, "Optimized gas pressure of an Rb vapor cell in a single-beam SERF magnetometer," Opt. Express **30**(1), 336–348 (2022).
36. K. James and J. Love, *Cooperative interactions in dense thermal Rb vapour conned in nm-scale cells* (Durham University, 2013), Chap. 1
37. S. Appelt, A. Ben-Amar Baranga, C. J. Erickson, *et al.*, "Theory of spin-exchange optical pumping of ^{3}He and ^{129}Xe," Phys. Rev. A **58**(2), 1412–1439 (1998).
38. W. J. Zheng, X. Bi, G. Y. Zhang, *et al.*, "Experimental demonstration of light narrowing effect based on free atomic spin precession," Chin. J. Laser **47**(3), 0304001 (2020).
39. S. Appelt, A. Ben-Amar Baranga, A. R. Young, *et al.*, "Light narrowing of rubidium magnetic-resonance lines in high-pressure optical-pumping cells," Phys. Rev. A **59**(3), 2078–2084 (1999).
40. Y.-Y. Jau, A. B. Post, N. N. Kuzma, *et al.*, "Intense, narrow atomic-clock resonances," Phys. Rev. Lett. **92**(11), 110801 (2004).

Optics EXPRESS

41. J. D. Li, W. Quan, B. Q. Zhou, *et al.*, "SERF atomic magnetometer–recent advances and applications: a aeview," IEEE Sensors J. **18**(20), 8198–8207 (2018).
42. K. Mouloudakis, J. Kong, A. Sierant, *et al.*, "Anomalous noise spectra in a spin-exchange-relaxation-free alkali-metal vapor," Phys. Rev. A **109**(4), L040802 (2024).